

# Raman Spectroscopic and DFT Study of COA-Cl and Its Analogues

Takayuki Umakoshi,\* Takumi Urakami, Haruki Kidoguchi, Keishi Yang, Prabhat Verma, Hirofumi Sato, Masahiro Higashi, and Ikuko Tsukamoto\*



Cite This: *J. Phys. Chem. A* 2023, 127, 1849–1856



Read Online

ACCESS |



Metrics & More

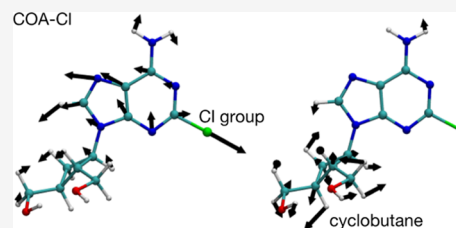


Article Recommendations



Supporting Information

**ABSTRACT:** COA-Cl is a newly synthesized adenosine analogue that exhibits various physiological activities. Its angiogenic, neurotropic, and neuroprotective potencies make it promising for the development of medicines. In this study, we show Raman spectroscopic study of COA-Cl to elucidate molecular vibrations and related chemical properties. Density functional theory calculations were combined with the Raman spectroscopic data to understand the details of each vibrational mode. Comparative analysis with adenine, adenosine, and other nucleic acid analogues enabled identification of unique Raman peaks originating from the cyclobutane moiety and chloro group of COA-Cl. This study provides fundamental knowledge and crucial insights for further development of COA-Cl and related chemical species.



## INTRODUCTION

COA-Cl is a recently synthesized novel adenosine analogue<sup>1</sup> that exerts strong angiogenic potency with the contribution of ERK1/2 activation,<sup>1</sup> sphingosine-1-phosphate receptor 1,<sup>2</sup> and enhanced vascular endothelial growth factor secretion.<sup>3</sup> COA-Cl also has neurotropic/protective potencies. The administration of COA-Cl to rodents reduced the damage caused by cerebral infarction,<sup>4</sup> cerebral hemorrhage,<sup>5</sup> myocardial infarction,<sup>6</sup> and spinal cord injury.<sup>7</sup> COA-Cl also improved the hippocampus-dependent learning of Alzheimer's disease model mice.<sup>8</sup> In phenochromocytoma 12 (PC12) cells, COA-Cl activates tyrosine hydroxylase, a key enzyme in catecholamine synthesis, and increases dopamine secretion. Enhanced dopamine secretion from dorsal striatum of living mice was also confirmed.<sup>9</sup> Furthermore, COA-Cl inhibited the transforming growth factor (TGF)- $\beta$ 1-induced epithelial–mesenchymal transition, which is related to cancer progression and organ fibrosis in RLD/Abca3 cells,<sup>10</sup> and COA-Cl also prevented TGF- $\beta$ 1-induced CTGF (connective tissue growth factor) expression in normal human dermal fibroblasts and attenuated skin fibrosis in mice models of systemic sclerosis.<sup>11</sup>

In this study, we show the Raman spectroscopic study of COA-Cl to elucidate its molecular vibrations. Density functional theory (DFT) is also employed to calculate the Raman spectra and analyze the molecular vibrational modes for each Raman peak. Comparative analyses of adenine, adenosine, and other nucleic acid analogues using Raman spectroscopy and DFT calculations reveal the detailed molecular vibrations of COA-Cl. This fundamental and thorough study provides deep insights into the Raman spectroscopic and molecular vibrational characteristics of COA-Cl, which should contribute to further development of COA-Cl and related chemical compounds. Understanding the physical and chemical proper-

ties of such a novel small molecule is essential for elucidating its fundamental properties and physiological activities.

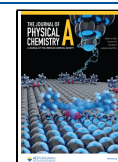
## METHODS AND MATERIALS

**Experimental Setup for Raman Measurements.** In this study, we utilized a homemade Raman spectroscope. Three single-mode continuous-wave lasers with different wavelengths were installed, with wavelengths of 442 (IK4401R-D, KIMON ELECTRIC), 532 (torus 532, Laser Quantum), and 633 nm (DL633-050-SO, CrystaLaser). The laser light was guided into an inverted optical microscope (Eclipse Ti2, Nikon) after passing through a beam expander, wave plates, and several filters. The powder samples were placed on the sample stage of the microscope. The incident lasers were focused on the samples through an oil-immersion objective lens (NA: 1.45,  $\times$ 100), and scattered signals were collected by the same objective in the back-scattering configuration. Strong Rayleigh-scattered light was effectively eliminated using a notch filter, and only Raman signals were guided into the spectroscope (IsoPlane 160, Teledyne). The signals were finally detected using a Peltier-cooled CCD camera (PIXIS\_100BRX, Teledyne). Further details are described in our earlier reports.<sup>12–15</sup> We have also tried to obtain Raman spectra with COA-Cl solution. However, the concentration of COA-Cl solution could not be high enough for Raman measurements because

**Received:** November 29, 2022

**Revised:** February 8, 2023

**Published:** February 21, 2023



the saturated concentration was as low as  $\sim 10$  mM. Clear Raman spectra were not obtained at this condition.

**Synthesis of COA-Cl and Derivatives.** COA-Cl was synthesized, as previously described.<sup>1</sup> COA-Cl is now commercially available from FUJIFILM WAKO Pure Chemical Corporation (Osaka, Osaka, Japan). Its analogues were synthesized according to methods reported in previous studies.<sup>16–18</sup>

**DFT Calculations.** To investigate the Raman spectra, DFT calculations were performed with the Gaussian 16 program package.<sup>19</sup> The B3LYP functional was employed with the aug-cc-pVDZ basis set. B3LYP was adopted because the obtained Raman spectra were in good agreement with the experimental spectra, compared with other functionals such as BLYP and  $\omega$ B97X-D. It is noted that the Raman spectra calculated with the aug-cc-pVDZ basis set were also in good agreement with those calculated with the larger aug-cc-pVTZ basis set.<sup>20</sup> For molecules with several conformations, the most stable conformers were used for analysis of the Raman spectra. No scaling factor was used for vibrational frequencies. To analyze the molecular vibrational modes, potential energy distribution analysis was performed using the VEDA program package (see the Supporting Information).<sup>21</sup>

## RESULTS

Figure 1a shows the molecular structure of COA-Cl (previously abbreviated as 2Cl-C. OXT-A; 6-amino-2-chloro-

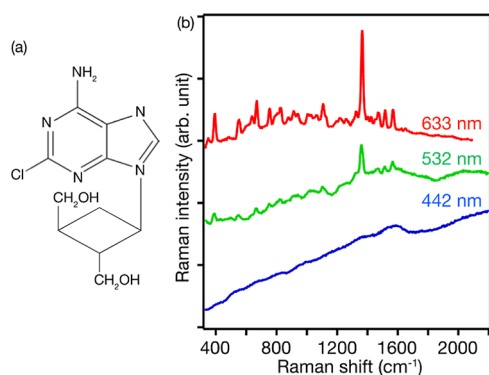


**Figure 1.** (a) Molecular structure of COA-Cl. (b) Raman spectra of COA-Cl obtained with different excitation wavelengths of 442, 532, and 633 nm.

9-[*trans-trans*-2',3'-bis(hydroxymethyl)cyclobutyl]-purine). The dependence of the Raman measurements on the excitation wavelength was evaluated to understand its influence on the Raman spectrum of COA-Cl and to determine a suitable wavelength for the Raman measurements. We used three lasers with wavelengths of 442, 532, and 633 nm. As shown in Figure 1b, the Raman spectra exhibited completely different features depending on the excitation wavelength. Multiple clear Raman peaks were obtained at a wavelength of 633 nm. In contrast, upon excitation at 442 nm, the Raman signals were completely overwhelmed by fluorescence noise due to autofluorescence from COA-Cl because the excitation wavelength was close to the absorption band of COA-Cl in the ultraviolet region. Although several Raman peaks were observed at an excitation wavelength of 532 nm, the signal-to-noise ratio was worse than that at the other wavelengths, and some peaks were not detected. The fluorescence noise degraded the Raman spectrum, even at a wavelength of 532 nm. Therefore, we

conclude that 633 nm is the most suitable wavelength for the Raman measurements of COA-Cl among these three wavelengths. The absorption bands of COA-Cl in the ultraviolet region were confirmed in the absorption spectrum as well as the calculated absorption coefficient in Figure S1 in the Supporting Information. As Raman spectrum of COA-Cl has never been obtained and investigated yet, we believe that the experimental verifications of basic characteristics of COA-Cl for Raman spectroscopic studies are crucial.

We then compared the Raman spectra of COA-Cl with those of adenine and adenosine. Adenine and adenosine have been extensively studied by Raman spectroscopy<sup>22–26</sup> and are expected to exhibit similar Raman spectroscopic characteristics as their molecular structures are similar to that of COA-Cl. Figure 2 shows the Raman spectra of adenine and adenosine.

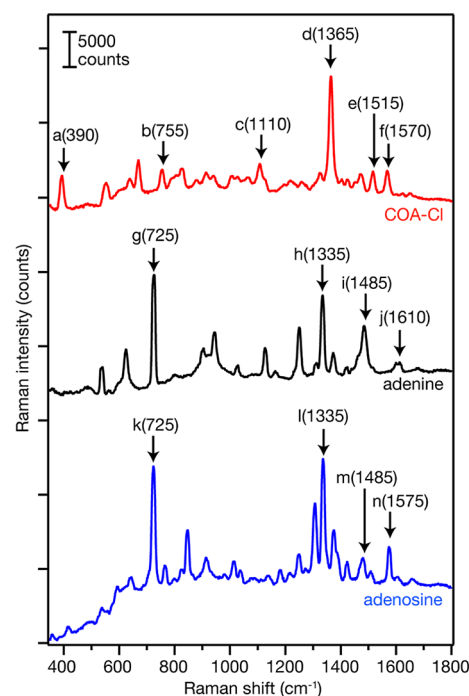


**Figure 2.** Raman spectra of COA-Cl, adenine, and adenosine, obtained at the excitation wavelength of 633 nm. The Raman spectrum of COA-Cl is the same as the red spectrum shown in Figure 1b.

The Raman spectrum of COA-Cl, which is the same as the red spectrum in Figure 1b, is also shown for comparison. Some representative Raman peaks are indicated by arrows, which are discussed in detail later. Similar features were observed in the spectra of adenine and adenosine. For example, the strong Raman peaks at approximately  $725\text{ cm}^{-1}$  (peaks g and k) and  $1335\text{ cm}^{-1}$  (peaks h and l) correspond well with each other. However, unexpectedly, none of the Raman peaks of COA-Cl correspond to those of either adenine or adenosine. A strong Raman peak was observed at approximately  $1365\text{ cm}^{-1}$  (peak d); however, it was slightly blue-shifted compared to peaks h and l. In addition, the strong Raman signal at  $\sim 725\text{ cm}^{-1}$  was not observed for COA-Cl.

To investigate the origin of each Raman peak, we calculated the Raman spectra and vibrational modes of each molecule using DFT (Figure 3). The calculated Raman spectra were in good agreement with the experimental results (Figure 2), which is important to validate that our DFT calculations were

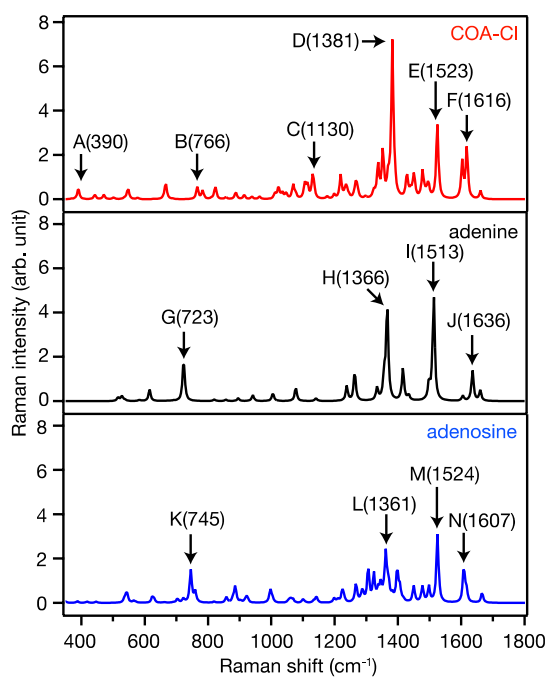


**Figure 3.** Raman spectra of COA-Cl, adenine, and adenosine, calculated at the B3LYP/aug-cc-pVTZ level.

implemented appropriately. The calculated Raman spectra of adenine and adenosine also agreed well with previous reports, which also verifies that our DFT calculations were performed correctly.<sup>25,26</sup> Note that one cannot expect the exact same Raman spectra for both calculation and experiment due to variations in the conditions under which the respective spectra are acquired. For example, a single isolated molecule is considered in DFT, whereas aggregated molecules in the powder form are analyzed experimentally. This difference can lead to slightly different results.

Figure 4a–c shows the molecular structures of COA-Cl, adenine, and adenosine, respectively, where a number was assigned to each atom to describe the vibrational modes. The representative Raman vibrational modes are listed in Tables 1–3. Some vibrational modes are illustrated in Figure 4d–k. The direction and length of the arrows indicate the direction and strength of the vibrations of each atom, respectively. Other vibrational modes are summarized in Figures S2–S4 in the Supporting Information as well as in Movie S1.

The strong Raman peak of COA-Cl at 1381  $\text{cm}^{-1}$  (peak D in Figure 4d) originated mainly from strong stretching vibrations inside the adenine moiety, especially between atoms 5, 9, 10, and 12. Strong C–H bending was also observed between atoms 1 and 2. The peaks at 1366  $\text{cm}^{-1}$  (peak H) for adenine and at 1361  $\text{cm}^{-1}$  (peak L) for adenosine also showed almost the same vibrational modes (Figure 4e,f). Although these vibrational modes are quite similar in the calculation, peak D of COA-Cl was slightly blue-shifted compared with peaks H and L. Therefore, we identified that the strongest Raman peak obtained as peak d in the experiment for COA-Cl originated from the same Raman modes as those for adenine and adenosine in peaks h and l. However, the peak position was slightly blue-shifted by  $\sim 30 \text{ cm}^{-1}$ , probably due to the cyclobutane moiety and the heavy chlorine atom on the adenine moiety. The calculated Raman spectra also show an enhancement in the Raman intensity, owing to the cyclobutane moiety and chlorine atom. Note that although the vibrational

mode in Figure 4f visually looks different from that in Figure 4d,e in the illustrations, Movie S1 shows that the vibrational modes of the adenine moiety of adenosine are similar with those of COA-Cl and adenine. Furthermore, we quantitatively evaluated the degrees of similarity between these vibrational modes in Tables S7 and S8 in the Supporting Information, where we discussed relatively lower similarity of peak L of adenosine (Figure 4f) to peak H of adenine (Figure 4e) in detail.

The other strong Raman peaks observed experimentally at approximately 725  $\text{cm}^{-1}$  (peaks g and k) for adenine and adenosine in Figure 2, which correspond to the peaks at 723 and 745  $\text{cm}^{-1}$  (peaks G and K) in the calculated spectra in Figure 3, were found to stem mostly from the breathing mode of the adenine moiety, as shown in Figure 4h,i. A similar vibrational mode was observed for COA-Cl at 766  $\text{cm}^{-1}$  (peak B), as shown in Figure 4g. However, the intensity of peak B was much lower than that of peaks G and K. The corresponding Raman peak in the experimental spectrum was also observed in almost the same position (peak b in Figure 2). Compared to adenine and adenosine, the peak position was blue-shifted to 755  $\text{cm}^{-1}$ , and the peak intensity was reduced, which agrees well with the calculation results. These comparisons indicate that the Raman peak (peak b) originating from the vibrational mode similar to the one contributing to the strong peaks (peaks g and k) of adenine and adenosine at  $\sim 725 \text{ cm}^{-1}$  was also observable in the spectrum of COA-Cl; however, the cyclobutane moiety and the chloro group in COA-Cl caused a blue shift to  $\sim 755 \text{ cm}^{-1}$  and intensity reduction of the breathing mode of the adenine moiety.

We also found that the vibrational modes at 1523  $\text{cm}^{-1}$  for COA-Cl (peak E), 1513  $\text{cm}^{-1}$  for adenine (peak I), and 1524  $\text{cm}^{-1}$  for adenosine (peak M) were almost identical, originating mainly from the combination of the stretching and bending modes of atoms 1, 2, 3, and 14 (see Supporting Information and Movie S1). The in-plane bending modes of atoms 6, 7, and 8 strongly contributed to this vibrational mode. In the experiment, peaks e, i, and m in Figure 2 most likely correspond to peaks E, I, and M, respectively. The vibrational modes at 1616  $\text{cm}^{-1}$  for COA-Cl (peak F), 1636  $\text{cm}^{-1}$  for adenine (peak J), and 1607  $\text{cm}^{-1}$  for adenosine (peak N) were also similar (see Supporting Information and Movie S1). For example, they are composed of strong stretching vibrations between atoms 5–9 and atoms 12–13. Peaks F, J, and N in the calculation also probably correspond to peaks f, j, and n in the experiment in Figure 2. We found that most of the vibrational modes were dominated by the adenine moiety, and the peak position and intensity for COA-Cl were slightly modified from those of adenine or adenosine due to the cyclobutane moiety and the chloro group.

In contrast, some vibrational modes are unique to COA-Cl. For example, the Raman peak at 390  $\text{cm}^{-1}$  (peak A) is mostly induced by the strong stretching vibration between C–Cl bonds (atoms 10–11), as shown in Figure 4j. In the experiment, we also observed a clear peak at 390  $\text{cm}^{-1}$  (peak a in Figure 2), which was not observed for adenine and adenosine. In addition, the vibrational mode at 1130  $\text{cm}^{-1}$  (peak C) was dominated by vibrations in the cyclobutane moiety, as shown in Figure 4k. We also observed a clear peak at a similar position to peak c in Figure 2. Although we also found small peaks at around 1130  $\text{cm}^{-1}$  for adenine and adenosine in Figure 3, which correspond to the peak position of 1141  $\text{cm}^{-1}$  for adenine and the peak position of 1142  $\text{cm}^{-1}$  for adenosine, we

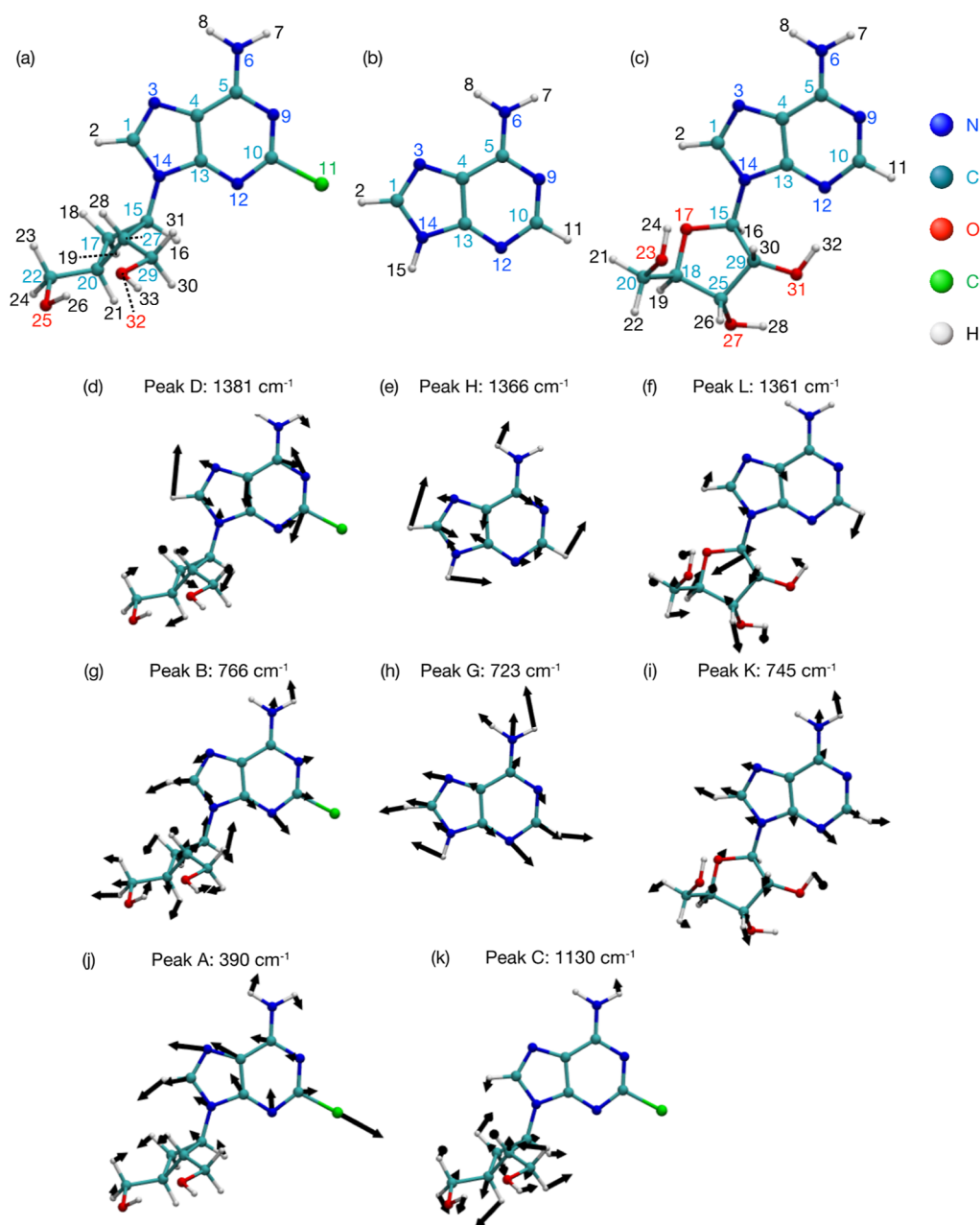


**Figure 4.** (a–c) Molecular structures of COA-Cl, adenine, and adenosine, respectively. An identical number is assigned to each atom to describe the molecular vibrational modes. (d–k) Schematics of representative molecular vibrational modes of COA-Cl, adenine, and adenosine.

confirmed these peaks were caused by completely different vibrational modes, as seen in Figures S3 and S4 in the Supporting Information. We revealed that these are unique Raman peaks for COA-Cl and are directly related to the molecular vibrations of the cyclobutane moiety and chloro group.

To further study the Raman spectrum of COA-Cl, we also investigated another COA-Cl analogue, C.OXT-A (6-amino-9-[*trans-trans*-2',3'-bis(hydroxymethyl) cyclobutyl]-purine). In C.OXT-A, the chlorine atom (atom 11) of COA-Cl is replaced with a hydrogen atom. Therefore, it is possible to investigate the effects of the chlorine atom by comparing the spectra of COA-Cl and C.OXT-A. Figure 5a shows the experimental Raman spectrum of C.OXT-A, and Figure 5b shows the Raman spectrum calculated using DFT. First, the unique peak in the spectrum of COA-Cl at  $390\text{ cm}^{-1}$  (peak a) disappeared

in that of C.OXT-A, as shown in Figure 5a. This was expected because this peak originates from the strong vibration of the chloro group. The peak should disappear when the chlorine atom is replaced with a hydrogen atom. This comparison further supports the fact that the peak observed at  $390\text{ cm}^{-1}$  in the experiment was attributed to the chlorine atom of COA-Cl. In addition, a strong peak was observed at approximately  $735\text{ cm}^{-1}$  (peak o), as shown in Figure 5a. This peak was also observed for adenine and adenosine, as shown in Figure 2. In contrast, the peak was significantly weakened and blue-shifted to  $\sim 755\text{ cm}^{-1}$  in the spectrum of COA-Cl. Thus, we evaluated the vibrational mode at peak O in Figure 5b, which is shown in Figure 5c. This shows the breathing mode of the adenine moiety, which is exactly the same as peaks G and K in Figure 4h,i. Therefore, we revealed that the reduced peak intensity and blue-shift of the peak position were mostly caused by the

**Table 1. Assignment of Representative Vibrational Modes of COA-Cl through DFT Calculations<sup>a</sup>**

wavenumber (cm <sup>-1</sup> )	Raman activity (Å <sup>4</sup> AMU <sup>-1</sup> )	assignment of vibrational modes
390	6.86	stretching of 10-11 and 12-13, in-plane bending of 10-12-13, 9-10-12, and 1-3-4
547	6.62	in-plane bending of 5-9-10 and 10-12-13, stretching of 5-6
666	10.93	in-plane bending of 9-10-12, 5-9-10, 10-12-13, and 3-1-14
766	8.09	in-plane bending of 1-14-13 and 9-10-12, stretching of 12-13 (breathing mode of the adenine moiety)
1130	15.86	stretching of 17-28, in-plane bending of 21-29-30, 22-24-25, and 15-19-17
1267	11.97	in-plane bending of 2-1-3, 14-1-3, and 5-6-7, stretching of 1-3 and 9-10
1381	117.66	stretching of 9-10 and 5-9, in-plane bending of 1-3-4, 3-1-14, and 2-1-3
1523	60.19	stretching of 1-3, in-plane bending of 2-1-3, 1-14-13, and 7-6-8
1616	41.45	stretching of 5-9 and 12-13, in-plane bending of 4-13-12 and 7-6-8

<sup>a</sup>In the assignment of the vibrational modes, the number indicates each atom of COA-Cl, as shown in Figure 4a.

**Table 2. Assignment of Representative Vibrational Modes of Adenine Theoretically through DFT Calculations<sup>a</sup>**

wavenumber (cm <sup>-1</sup> )	Raman activity (Å <sup>4</sup> AMU <sup>-1</sup> )	assignment of vibrational modes
528	0.72	in-plane bending of 10-12-13, 5-9-10, and 4-13-12
616	7.46	in-plane bending between 9-10-12, 1-14-13, 5-9-10, and 10-12-13
723	27.88	stretching of 12-13, in-plane bending of 1-14-13 and 5-9-10. (breathing mode of the adenine moiety)
1077	9.66	stretching of 1-14, in-plane bending of 1-14-15 and 2-1-3
1264	21.60	in-plane bending of 2-1-3 and 1-14-15, stretching of 1-3 and 9-10
1366	72.46	stretching of 5-9 and 1-14, in-plane bending of 1-3-4, 3-1-14, and 2-1-3
1513	81.77	stretching of 1-3 and 12-13, in-plane bending of 2-1-3, 1-14-13, and 7-6-8
1636	24.28	stretching of 5-9 and 12-13, in-plane bending of 4-13-12 and 1-14-15

<sup>a</sup>In the assignment of vibrational modes, the number indicates each atom of adenine, as shown in Figure 4b.

chlorine atom in COA-Cl rather than the cyclobutane moiety. We also confirmed the vibrational mode of the cyclobutane moiety in the spectrum of C.OXT-A at 1130 cm<sup>-1</sup> (peak P) (Figure 5d), which is the same as that of COA-Cl, as shown in Figure 4k. However, this was not observed in the experiment, as shown in Figure 5a, the reason for which is still under investigation. As previously mentioned, the calculation did not perfectly match the experimental results. We suspect that the peak was weakened and embedded in the noise level in the experiment because it was inherently not a strong Raman signal. COA-Cl has very strong angiogenic potency, but this potency completely disappears when the chloro group is removed.<sup>1</sup> The presence of the chloro group of COA-Cl is critical for imparting physiological activities. The difference in the Raman spectra of COA-Cl and C.OXT-A indicates the role

**Table 3. Assignment of Representative Vibrational Modes of Adenosine through DFT Calculations<sup>a</sup>**

wavenumber (cm <sup>-1</sup> )	Raman activity (Å <sup>4</sup> AMU <sup>-1</sup> )	assignment of vibrational modes
543	6.74	stretching of 29-31 and 18-20, in-plane bending of 18-25-29 and 27-25-29
745	21.68	torsion of 15-29-31-32, stretching of 12-13, in-plane bending of 1-14-13 and 5-9-10 (breathing mode of the adenine moiety)
886	11.17	stretching of 18-20 and 20-23, out-of-plane bending of 18-17-25-20, torsion of 15-17-18-25
1267	14.07	in-plane bending of 2-1-3, 14-1-3, and 5-6-7, stretching of 9-10 and 14-15
1361	34.22	in-plane bending of 16-15-17, 17-18-19, 20-23-24, 3-1-14, and 1-3-4, stretching of 1-14 and 5-9
1524	53.92	stretching of 1-3 and 13-14, in-plane bending of 2-1-3, 1-14-13, and 7-6-8
1615	41.45	in-plane bending of 7-6-8, 1-13-14, and 1-3-4, stretching of 12-13 and 9-10

<sup>a</sup>In the assignment of vibrational modes, the number indicates each atom of adenosine, as shown in Figure 4c.

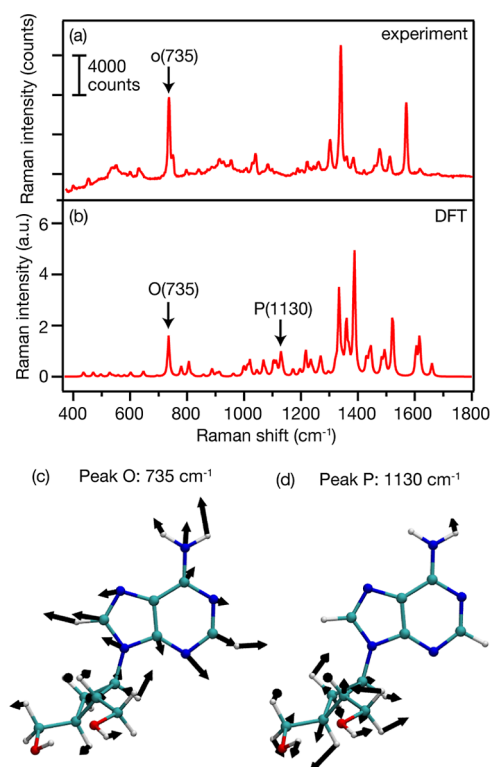


**Figure 5.** (a) Raman spectrum of C.OXT-A, (b) calculated Raman spectrum of C.OXT-A at the B3LYP/aug-cc-pVTZ level. (c) Schematic of the vibrational mode of C.OXT-A at 735 cm<sup>-1</sup>. (d) Schematic of the vibrational mode of C.OXT-A at 1130 cm<sup>-1</sup>.

of the chloro group. Further molecular vibrational studies will provide more information regarding this issue.

Finally, we calculated the Raman spectra of chloro-adenine and chloro-adenosine for comparison with that of COA-Cl (Figure 6a,b). Here, the hydrogen atom (atom 11) of adenine and adenosine was replaced by a chlorine atom. Compared to the calculated Raman spectra of adenine and adenosine in Figure 3, owing to the added chlorine atom, the spectral shapes became slightly similar to that of COA-Cl. As expected, Raman

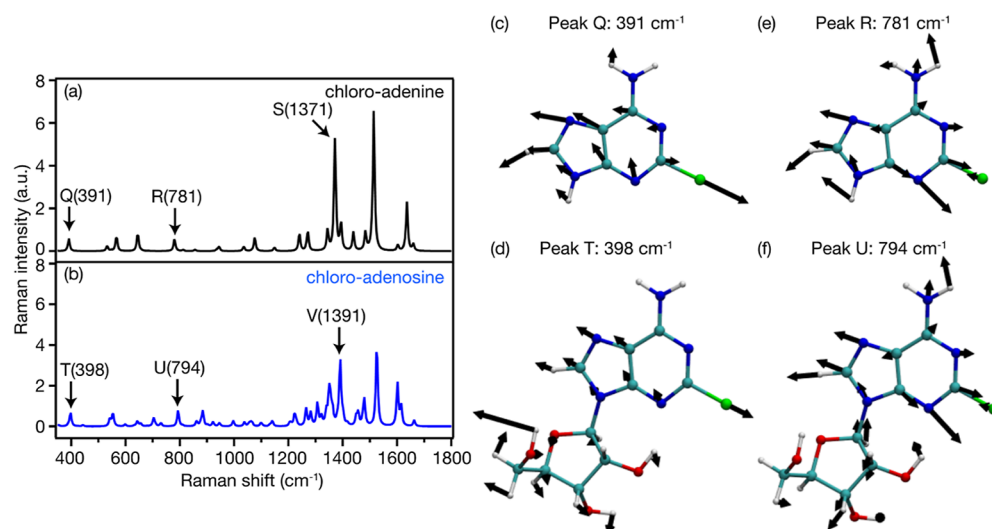


**Figure 6.** (a) Calculated Raman spectrum of chloro-adenine, (b) calculated Raman spectrum of chloro-adenosine, (c) schematic of the vibrational mode of chloro-adenine at  $391\text{ cm}^{-1}$ , (d) schematic of the vibrational mode of chloro-adenosine at  $398\text{ cm}^{-1}$ , (e) schematic of the vibrational mode of chloro-adenine at  $781\text{ cm}^{-1}$ , and (f) schematic of the vibrational mode of chloro-adenosine at  $794\text{ cm}^{-1}$ .

peaks were observed at  $\sim 390\text{ cm}^{-1}$  (peaks Q and T) in both spectra because of the strong vibration of the chloro group, which was confirmed in the vibrational modes shown in Figure 6c,d. Moreover, the strong peaks observed at  $723\text{ cm}^{-1}$  (peak G) for adenine and  $745\text{ cm}^{-1}$  (peak K) for adenosine in Figure 3 were blue-shifted to  $781\text{ cm}^{-1}$  (peak R) and  $794\text{ cm}^{-1}$  (peak U), respectively. In addition, the peak intensities were largely reduced. These peaks originate from the breathing mode of the adenine moiety, as shown in Figure 6e,f. A blue shift and intensity decrease of this breathing mode were also observed for COA-Cl (peak B). Therefore, we concluded that this change in the breathing mode of the adenine moiety was caused by chlorine atoms. The strong peak D of COA-Cl was also blue-shifted compared to peak H of adenine and peak L of adenosine in Figure 3, even though the origins of these peaks are the same vibrational modes. Similarly, peak H at  $1366\text{ cm}^{-1}$  for adenine was blue-shifted to  $1371\text{ cm}^{-1}$  for chloro-adenine (peak S), and the peak at  $1366\text{ cm}^{-1}$  for adenosine was blue-shifted to  $1391\text{ cm}^{-1}$  for chloro-adenosine (peak V) (see the Supporting Information for the vibrational modes). Overall, we revealed that such a heavy chlorine atom has a large influence on the Raman vibrational modes, which results in a large difference in the Raman spectrum of COA-Cl compared to those of adenine and adenosine.

## CONCLUSIONS

The Raman characteristics of COA-Cl were extensively investigated through both experiments and DFT calculations to elucidate the molecular vibrations and its related chemical properties. COA-Cl exhibits multiple clear Raman peaks. The Raman spectrum of COA-Cl differs from those of adenine and adenosine, although the molecular structures are similar. Through thorough studies on the Raman spectrum of COA-Cl and comparison with adenine, adenosine, and other analogues, we identified the vibrational modes of the experimentally obtained Raman peaks of COA-Cl. We reveal that COA-Cl indeed possesses similar molecular vibrational modes to adenine and adenosine; however, the peak intensities and peak positions are modified by the cyclobutane moiety and the chloro group of COA-Cl. These effects of the chlorine

atom and the cyclobutane moiety on molecular vibrations were revealed by comparing COA-Cl with adenine, adenosine, and other analogues, which was not possible by analyzing COA-Cl only. In particular, the fact that the heavy chlorine atom has a significant influence on the Raman characteristics of COA-Cl is essential to understand chemical and physiological properties of COA-Cl, which implies the unique molecular vibrations caused by the chlorine atom might play a crucial role for COA-Cl to gain its superior chemical properties. We believe that this Raman spectroscopic study provides novel insights into structure–activity relationships of COA-Cl. Additional information on almost all the vibrational modes is provided in detail in the Supporting Information. The fundamental properties reported in this study are crucial and beneficial for the further development of COA-Cl and related chemical compounds.

## ASSOCIATED CONTENT

### Supporting Information

The Supporting Information is available free of charge at <https://pubs.acs.org/doi/10.1021/acs.jpca.2c08382>.

Absorption spectrum of COA-Cl, schematics of molecular vibrational modes, molecular vibration motions, potential energy distribution analysis of vibrational modes, and quantitative analysis of similarity between vibrational modes (PDF)

Molecular vibration modes of COA-Cl, adenine, adenosine 1, C.OXT-A, chloro-adenine, and chloro-adenosine (MP4)

## AUTHOR INFORMATION

### Corresponding Authors

Takayuki Umakoshi – *Institute for Advanced Co-Creation Studies and Department of Applied Physics, Osaka University, Suita, Osaka 565-0871, Japan; PRESTO, Japan Science and Technology Agency, Kawaguchi, Saitama 332-0012, Japan;* [orcid.org/0000-0002-0479-1124](https://orcid.org/0000-0002-0479-1124); Email: [umakoshi@ap.eng.osaka-u.ac.jp](mailto:umakoshi@ap.eng.osaka-u.ac.jp)

Ikuko Tsukamoto – *Department of Pharmaco-Bio-Informatics, Faculty of Medicine, Kagawa University,*

Takamatsu, Kagawa 761-0793, Japan;  
Email: tsukamoto.ikuko@kagawa-u.ac.jp

## Authors

**Takumi Urakami** – Department of Molecular Engineering, Graduate School of Engineering, Kyoto University, Kyoto 615-8510, Japan

**Haruki Kidoguchi** – Department of Applied Physics, Osaka University, Suita, Osaka 565-0871, Japan

**Keishi Yang** – Department of Applied Physics, Osaka University, Suita, Osaka 565-0871, Japan

**Prabhat Verma** – Department of Applied Physics, Osaka University, Suita, Osaka 565-0871, Japan; [orcid.org/0000-0002-7781-418X](https://orcid.org/0000-0002-7781-418X)

**Hirofumi Sato** – Department of Molecular Engineering, Graduate School of Engineering, Kyoto University, Kyoto 615-8510, Japan; Fukui Institute for Fundamental Chemistry, Kyoto University, Kyoto 606-8103, Japan; [orcid.org/0000-0001-6266-9058](https://orcid.org/0000-0001-6266-9058)

**Masahiro Higashi** – Department of Molecular Engineering, Graduate School of Engineering, Kyoto University, Kyoto 615-8510, Japan; [orcid.org/0000-0001-9829-389X](https://orcid.org/0000-0001-9829-389X)

Complete contact information is available at:  
<https://pubs.acs.org/10.1021/acs.jpca.2c08382>

## Author Contributions

Takayuki Umakoshi, H.K., and K.Y. implemented the experiments and analyzed the results. Takumi Urakami and M.H. performed the calculations and analyzed the results. Takayuki Umakoshi and I.T. conceived and designed this project. Takayuki Umakoshi, P.V., H.S., M.H., and I.T. supervised this research. Takayuki Umakoshi, M.H., and I.T. wrote the manuscript. All authors contributed to the discussion and finalization of the manuscript.

## Notes

The authors declare no competing financial interest.

## ACKNOWLEDGMENTS

This work was supported in part by JSPS KAKENHI grant number 20H02658, JSPS KAKENHI grant number JP20H05839, and JST PRESTO grant number JPMJPR19G2. Theoretical computations were partly performed using the Research Center for Computational Science, Okazaki, Japan (22-IMS-C021).

## REFERENCES

- (1) Tsukamoto, I.; Sakakibara, N.; Maruyama, T.; Igarashi, J.; Kosaka, H.; Kubota, Y.; Tokuda, M.; Ashino, H.; Hattori, K.; Tanaka, S.; et al. A Novel Nucleic Acid Analogue Shows Strong Angiogenic Activity. *Biochem. Biophys. Res. Commun.* **2010**, *399*, 699–704.
- (2) Igarashi, J.; Hashimoto, T.; Kubota, Y.; Shoji, K.; Maruyama, T.; Sakakibara, N.; Takuwa, Y.; Ujihara, Y.; Katanosaka, Y.; Mohri, S.; et al. Involvement of S1P1 Receptor Pathway in Angiogenic Effects of a Novel Adenosine-like Nucleic Acid Analog COA-Cl in Cultured Human Vascular Endothelial Cells. *Pharmacol. Res. Perspect.* **2014**, *2*, No. e00068.
- (3) Igarashi, J.; Okamoto, R.; Yamashita, T.; Hashimoto, T.; Karita, S.; Nakai, K.; Kubota, Y.; Takata, M.; Yamaguchi, F.; Tokuda, M.; et al. A Key Role of PGC-1 $\alpha$  Transcriptional Coactivator in Production of VEGF by a Novel Angiogenic Agent COA-Cl in Cultured Human Fibroblasts. *Physiol. Rep.* **2016**, *4*, No. e12742.
- (4) Okabe, N.; Nakamura, E.; Himi, N.; Narita, K.; Tsukamoto, I.; Maruyama, T.; Sakakibara, N.; Nakamura, T.; Itano, T.; Miyamoto, O. Delayed Administration of the Nucleic Acid Analog 2Cl-C.OXT-A

Attenuates Brain Damage and Enhances Functional Recovery after Ischemic Stroke. *Brain Res.* **2013**, *1506*, 115–131.

(5) Lu, F.; Nakamura, T.; Okabe, N.; Himi, N.; Nakamura-Maruyama, E.; Shiromoto, T.; Narita, K.; Tsukamoto, I.; Xi, G.; Keep, R. F.; et al. COA-Cl, a Novel Synthesized Nucleoside Analog, Exerts Neuroprotective Effects in the Acute Phase of Intracerebral Hemorrhage. *J. Stroke Cerebrovasc. Dis.* **2016**, *25*, 2637–2643.

(6) Nishikido, T.; Oyama, J.; Shiraki, A.; Tsukamoto, I.; Igarashi, J.; Node, K. COA-Cl (2-Cl-C.OXT-A, K. Can Promote Coronary Collateral Development Following Acute Myocardial Infarction in Mice. *Sci. Rep.* **2019**, *9*, 2533.

(7) Sakamoto, I.; Himi, N.; Hayashi, N.; Okabe, N.; Nakamura-Maruyama, E.; Tsukamoto, I.; Hasegawa, T.; Miyamoto, O. The Protective Effect and Mechanism of COA-Cl in Acute Phase after Spinal Cord Injury. *Neurosci. Res.* **2021**, *170*, 114–121.

(8) Kishimoto, Y.; Tsukamoto, I.; Nishigawa, A.; Nishimoto, A.; Kirino, Y.; Kato, Y.; Konishi, R.; Maruyama, T.; Sakakibara, N. Data on COA-Cl Administration to the APP/PS2 Double-Transgenic Mouse Model of Alzheimer's Disease: Improved Hippocampus-Dependent Learning and Unchanged Spontaneous Physical Activity. *Data Brief* **2018**, *20*, 1877–1883.

(9) Jamal, M.; Tsukamoto, I.; Takata, M.; Ito, A.; Tanaka, N.; Miki, T.; Takakura, A.; Ameno, K.; Kubota, Y.; Konishi, R.; et al. COA-Cl Induces Dopamine Release and Tyrosine Hydroxylase Phosphorylation: In Vivo Reverse Microdialysis and in Vitro Analysis. *Brain Res.* **2019**, *1706*, 68–74.

(10) Kawami, M.; Deguchi, J.; Yumoto, R.; Sakakibara, N.; Tsukamoto, I.; Konishi, R.; Takano, M. Effect of COA-Cl on Transforming Growth Factor-B1-Induced Epithelial-mesenchymal Transition in RLE/Abca3 Cells. *Drug Metab. Pharmacokinet.* **2017**, *32*, 224–227.

(11) Nakai, K.; Karita, S.; Igarashi, J.; Tsukamoto, I.; Hirano, K.; Kubota, Y. COA-Cl Prevented TGF-B1-Induced CTGF Expression by Akt Dephosphorylation in Normal Human Dermal Fibroblasts, and It Attenuated Skin Fibrosis in Mice Models of Systemic Sclerosis. *J. Dermatol. Sci.* **2019**, *94*, 205–212.

(12) Moriyama, T.; Umakoshi, T.; Hattori, Y.; Taguchi, K.; Verma, P.; Kitamura, M. Polarization Raman Imaging of Organic Monolayer Islands for Crystal Orientation Analysis. *ACS Omega* **2021**, *6*, 9520–9527.

(13) Umakoshi, T.; Taniguchi, M.; Verma, P. Anharmonic Effects in Single-Walled Carbon Nanotubes Analyzed through Low-Temperature Raman Imaging. *J. Phys. Chem. C* **2020**, *124*, 6922–6928.

(14) Sam, R. T.; Umakoshi, T.; Verma, P. Probing Stacking Configurations in a Few Layered MoS<sub>2</sub> by Low Frequency Raman Spectroscopy. *Sci. Rep.* **2020**, *10*, 21227.

(15) Umakoshi, T.; Kawashima, K.; Moriyama, T.; Kato, R.; Verma, P. Tip-Enhanced Raman Spectroscopy with Amplitude-Controlled Tapping-Mode AFM. *Sci. Rep.* **2022**, *12*, 12776.

(16) Maruyama, T.; Sakakibara, N.; Tsukamoto, I.; Tsuruta, T.; Takata, M.; Konishi, R.; Maruyama, T. Novel Synthesis of Carbocyclic Oxetanocin Analogs (2-Alkoxy-C.OXT-A) and Their Tube Formation Activities of Human Umbilical Vein Endothelial Cells (HUVEC). *Heterocycles* **2012**, *85*, 1105–1116.

(17) Sakakibara, N.; Igarashi, J.; Takata, M.; Konishi, R.; Suzue, N.; Kato, Y.; Maruyama, T.; Tsukamoto, I. Design, Synthesis, and Evaluation of Novel 2-Halogenated or Aminated Carbocyclic Oxetanocin Analogs as Potential Angiogenic Agents. *Heterocycles* **2015**, *91*, 1823.

(18) Sakakibara, N.; Igarashi, J.; Takata, M.; Demizu, Y.; Misawa, T.; Kurihara, K.; Konishi, R.; Kato, Y.; Maruyama, T.; Tsukamoto, I. Synthesis and Evaluation of Novel Carbocyclic Oxetanocin A (COA-Cl) Derivatives as Potential Tube Formation Agents. *Chem. Pharm. Bull.* **2015**, *63*, 701–709.

(19) Frisch, M. J.; Trucks, G. W.; Schlegel, H. B.; Scuseria, G. E.; Robb, M. A.; Cheeseman, J. R.; Scalmani, G.; Barone, V.; Petersson, G. A.; Nakatsuji, H.; Li, X.; Caricato, M.; Marenich, A. V.; Bloino, J.; Janesko, B. G.; Gomperts, R.; Mennucci, B.; Hratchian, H. P.; Ortiz, J. V.; Izmaylov, A. F.; Sonnenberg, J. L.; Williams-Young, D.; Ding, F.;

Lipparini, F.; Egidi, F.; Goings, J.; Peng, B.; Petrone, A.; Henderson, T.; Ranasinghe, D.; Zakrzewski, V. G.; Gao, J.; Rega, N.; Zheng, G.; Liang, W.; Hada, M.; Ehara, M.; Toyota, K.; Fukuda, R.; Hasegawa, J.; Ishida, M.; Nakajima, T.; Honda, Y.; Kitao, O.; Nakai, H.; Vreven, T.; Throssell, K.; Montgomery, J. A., Jr.; Peralta, J. E.; Ogliaro, F.; Bearpark, M. J.; Heyd, J. J.; Brothers, E. N.; Kudin, K. N.; Staroverov, V. N.; Keith, T. A.; Kobayashi, R.; Normand, J.; Raghavachari, K.; Rendell, A. P.; Burant, J. C.; Iyengar, S. S.; Tomasi, J.; Cossi, M.; Millam, J. M.; Klene, M.; Adamo, C.; Cammi, R.; Ochterski, J. W.; Martin, R. L.; Morokuma, K.; Farkas, O.; Foresman, J. B.; Fox, D. J. *Gaussian 16*, Revision C.01; Gaussian, Inc.: Wallingford CT, 2016.

(20) Cheeseman, J. R.; Frisch, M. J. Basis Set Dependence of Vibrational Raman and Raman Optical Activity Intensities. *J. Chem. Theory Comput.* **2011**, *7*, 3323–3334.

(21) Jamroz, M. H. *Vibrational Energy Distribution Analysis VEDA 4*; ScienceOpen, Inc.: Warsaw, 2004.

(22) Hirakawa, A. Y.; Okada, H.; Sasagawa, S.; Tsuboi, M. Infrared and Raman Spectra of Adenine and Its 15N and 13C Substitution Products. *Spectrochim. Acta, Part A* **1985**, *41*, 209–216.

(23) Lee, S. A.; Anderson, A.; Smith, W.; Griffey, R. H.; Mohan, V. Temperature-Dependent Raman and Infrared Spectra of Nucleosides. Part I - Adenosine. *J. Raman Spectrosc.* **2000**, *31*, 891–896.

(24) Watanabe, H.; Ishida, Y.; Hayazawa, N.; Inouye, Y.; Kawata, S. Tip-Enhanced near-Field Raman Analysis of Tip-Pressurized Adenine Molecule. *Phys. Rev. B: Condens. Matter Mater. Phys.* **2004**, *69*, 155418.

(25) Giese, B.; McNaughton, D. Surface-Enhanced Raman Spectroscopic and Density Functional Theory Study of Adenine Adsorption to Silver Surfaces. *J. Phys. Chem. B* **2002**, *106*, 101–112.

(26) Sundin, E. M.; Ciubuc, J. D.; Bennet, K. E.; Ochoa, K.; Manciu, F. S. Comparative Computational and Experimental Detection of Adenosine Using Ultrasensitive Surface-Enhanced Raman Spectroscopy. *Sensors* **2018**, *18*, 2696.

## Recommended by ACS

### Electronic State Spectroscopy of Nitromethane and Nitroethane

Luiz V. S. Dalagnol, Paulo Limão-Vieira, *et al.*

FEBRUARY 02, 2023  
THE JOURNAL OF PHYSICAL CHEMISTRY A

READ 

### Heavy Metal Accumulation and Source Apportionment in Urban River under Ecological Restoration: Relationships with Land Use and Risk Assessment Based on Monte Carl...

Xi Gao, Jie Zeng, *et al.*

FEBRUARY 28, 2023  
ACS EARTH AND SPACE CHEMISTRY

READ 

### Temperature and Pressure Dependence of the Reaction between Ethyl Radical and Molecular Oxygen: Experiments and Master Equation Simulations

Timo T. Pekkanen, Arkke J. Eskola, *et al.*

JANUARY 25, 2023  
THE JOURNAL OF PHYSICAL CHEMISTRY A

READ 

### Triatomic Photoassociation in an Ultracold Atom–Molecule Collision

Ahmed A. Elkamshishy and Chris H. Greene

DECEMBER 30, 2022  
THE JOURNAL OF PHYSICAL CHEMISTRY A

READ 

Get More Suggestions >